Colloidal Nanoparticles for Intermediate Band Solar Cells

Márton Vörös,*,†,‡ Giulia Galli,*,‡,# and Gergely T. Zimanyi*,†

†Department of Physics, University of California, Davis, California 95616, United States, ‡Institute for Molecular Engineering, University of Chicago, Chicago, Illinois 60637, United States, and #Argonne National Laboratory, Lemont, Illinois 60439, United States

ABSTRACT The Intermediate Band (IB) solar cell concept is a promising idea to transcend the Shockley–Queisser limit. Using the results of first-principles calculations, we propose that colloidal nanoparticles (CNPs) are a viable and efficient platform for the implementation of the IB solar cell concept. We focused on CdSe CNPs and we showed that intragap states present in the isolated CNPs with reconstructed surfaces combine to form an IB in arrays of CNPs, which is well separated from the valence and conduction band edges. We demonstrated that optical transitions to and from the IB are active. We also showed that the IB can be electron doped in a solution, *e.g.*, by decamethylcobaltocene, thus activating an IB-induced absorption process. Our results, together with the recent report of a nearly 10% efficient CNP solar cell, indicate that colloidal nanoparticle intermediate band solar cells are a promising platform to overcome the Shockley–Queisser limit.

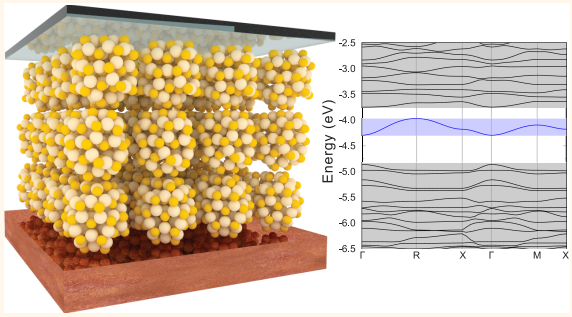

KEYWORDS: nanocrystal · nanoparticle solid · intermediate band · solar cell · density functional theory · doping · absorption

The maximum theoretical efficiency of conventional single junction bulk solar cells is limited to 33% (Shockley–Queisser (SQ) limit[1]) by two main factors: photons with subgap energies cannot be absorbed, and electron–hole pairs that were excited above the band gap by high-energy photons decay by emitting phonons, thereby heating the solar cell. Several ideas have been put forward to transcend the SQ limit, including up-conversion and down-conversion approaches.[2] The former involves capturing the subgap photons,[3−6] while the latter attempts to prevent thermalization of excited electron–hole pairs.[7,8]

A leading up-conversion proposal is to absorb subgap photons by an intermediate band (IB), formed within the band gap of the absorber.[4] Other proposals include absorption by impurity states.[5,6] The optimal value of the gap in an IB cell was determined to be about 2.4 eV for one-sun, and 1.93 eV under full concentration. With an appropriately positioned IB, the efficiency of an IB solar cell may rise well above the SQ limit: 49.4% at one-sun and 63.1% under full concentration.[4,9]

A down-conversion proposal that received widespread attention is the Multiple Exciton Generation (MEG) paradigm. It was advocated that MEG may be particularly efficient in nanoparticle absorbers.[7] When this expectation was experimentally verified,[10,11] it paved the way for the use of colloidal nanoparticles for solar energy conversion.[12−20]

Here, we propose adopting colloidal nanoparticles with IB bands for up-conversion processes. The IB scheme was mostly realized in epitaxial quantum dots (EQD) embedded in multilayer heterostructures,[21,22] where one or more intragap state(s), well separated from the conduction and the valence bands of the epilayers, may be found. The benefit of up-conversion in EQD-IB cells was unambiguously confirmed by observing an increase of the subgap absorption.[23−25] Other approaches to IB solar cells included heavy doping of bulk absorbers.[26−28]

While these results demonstrate the great promise of the intermediate band concept, exploiting IBs in epitaxial systems faces challenges. In particular: (i) The surface density of epitaxial quantum dots is

* Address correspondence to vormar@gmail.com, gagalli@uchicago.edu, zimanyi@physics.ucdavis.edu.

Received for review January 15, 2015 and accepted June 4, 2015.

Published online June 04, 2015
10.1021/acsnano.5b00332

presently limited to (4−6) × 10^{10}/cm^2,[22−25] which for ≈10 nm epilayer separation[24,25] and typical epitaxial QD dimensions of 30 × 30 × 7 nm^3 results in an absorbing volume fraction of 20−25%. Typically, 10−20 quantum dot epilayers need to be formed to reach even modest absorption increases compared to systems without the dots. (ii) QD−QD separations as wide as 10−15 nm were reported. Forming an intermediate band from the individual intragap states of the widely separated QDs is challenging.[21] (iii) Fabrication of epitaxial QDs requires a large number of device processing steps, with substantial cost-implications.[23−25] The (i)−(iii) challenges of the EQD with IB bands served as a major motivation to develop alternative implementations of the intermediate band concept.

In this Article, using the results of *ab initio* calculations, we propose that colloidal nanoparticles are a promising platform for implementing the IB concept in solar cells. In colloidal nanoparticles (CNPs), various mechanisms are known to form states with energy separated from those of the NP highest occupied molecular orbital (HOMO) and lowest unoccupied molecular orbital (LUMO). These mechanisms include (a) surface reconstruction,[17] (b) the presence of an interface in core/shell CNP,[29] (c) deep-level doping, such as Mn in CdSe NPs,[30] and (d) using a bidisperse mixture of CNPs.[31]

CNP absorbers offer several advantages over EQDs. CNPs fill a large fraction of the absorber as they can be closely packed,[32] resulting in an absorbing volume fraction substantially higher than that of EQDs. In addition, the synthesis of CNPs is a low temperature solution-based process. Thus, forming even a large number of CNP layers requires only a few process steps at low temperatures, substantially reducing energy-demand and cost. Finally, the CNP−CNP distance may be tuned by ligand engineering down to the sub-nanometer to nanometer regime,[32,33] and thus, the formation of an IB from the states of individual CNPs can in principle be controlled.

We focused our analysis on CdSe CNPs as a platform for CNPIB solar cells because of their suitable gap value. In accord with earlier results,[34] we found that surface reconstruction and quantum confinement generated a state with an energy well-separated from the HOMO and LUMO levels of the NP. In the following, such a state will be referred to as intragap state. From existing reports we identified reducing agents that are capable of electron-doping this intragap state.[35−37] We then considered arrays of CdSe CNPs, and computed their total energies and electronic structure from first-principles calculations. As expected, these arrays exhibited an intermediate band formed by the NPs' intragap states and we suggest that chemical-doping or photodoping may activate the IB-mediated absorption processes necessary for the operation of solar cells. Our paper also includes a qualitative estimate of the overall efficiency of these CNPIB solar cells. While several factors can only be known approximately, our estimate promises efficiencies in excess of 40%.

We suggest that the use of the CNPIB paradigm is timely, since very recently colloidal nanoparticle solar cells were demonstrated with efficiencies approaching 9%,[38] and 10%.[39] These breakthroughs prove the maturity and readiness of CNP technology. Nanoparticle solar cell efficiencies are today where organic solar cells were only three years ago.

We note that an idea related to our proposal has been recently put forward by Mendes *et al.*[40] However, in that design, only the IB states are localized on the CNP, while the valence band (VB) and conduction band (CB) states reside on an embedding host matrix. Since such host matrix plays an active role in the absorption, several additional factors need to be *simultaneously* optimized, making the design challenging. One of such challenges, *i.e.*, ensuring the proper band alignment between the CNP and the host, was highlighted recently.[41] We also note that the focus of ref 40 is on the addition of metal particles to boost the absorption through plasmonic effects.[42]

RESULTS AND DISCUSSION

First, we identified CNPs that are optimal platforms for implementing an IB concept for solar cells. A leading criterion for all nonconcentrating IB solar cells is that the optimal gap should be ≈2.4 eV. This criterion excludes some of the widely studied NPs, such as Pb(S,Se). On the other hand, CdSe appears to be a good candidate: the bulk band gap is ≈1.8 eV, widening into the optimal range in NP, as their diameter is reduced to ≈3 nm.[43,44]

Intragap State Formation. We started by carving spherical stoichiometric NPs out of the bulk wurtzite CdSe structure. Several starting configurations were generated by adding small random displacements (<0.5 Å) to the positions of Cd and Se atoms without imposing any symmetry. The NP geometries were then relaxed to their closest local minimum. The largest NP considered here, with formula $Cd_{45}Se_{45}$, has a diameter of about 1.5 nm.

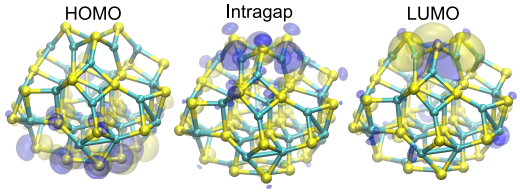

Figure 1. Ball and stick representation of the $Cd_{33}Se_{33}$ NP (cyan and yellow spheres represent cadmium and selenium atoms, respectively) and the isosurfaces of its HOMO, intragap and LUMO wave functions. Yellow (blue) isosurfaces represent positive (negative) isovalues of the electronic states.

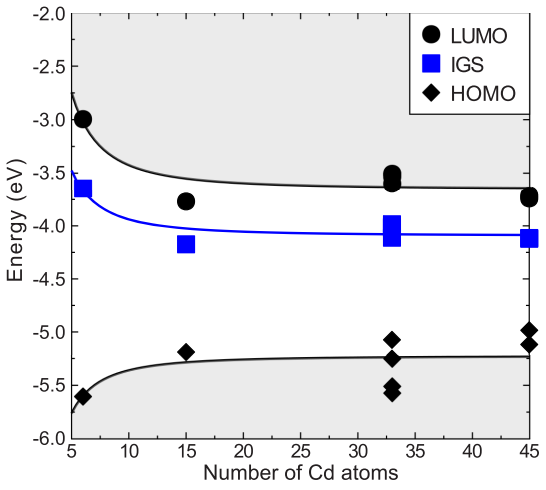

Figure 2. Single particle energies of the LUMO, intragap (IGS), and HOMO states of CdSe nanoparticles, as a function of the number of atoms in the NP. Energies refer to the vacuum level and were obtained at the DFT-PBE level of theory.

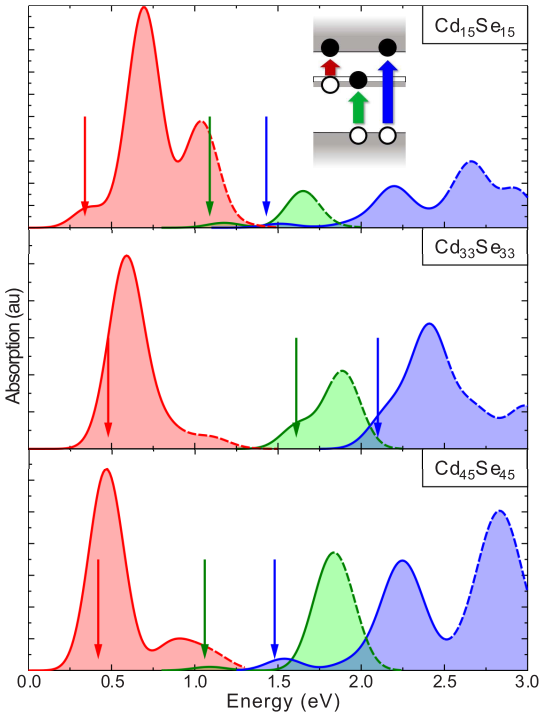

Figure 3. Absorption spectra of several NPs computed in the independent particle approximation (see Supporting Information for details). Red/green/blue curves correspond to (intragap state (IGS))→(LUMO+*X*)/(HOMO−*X*)→IGS/(HOMO−*X*)→(LUMO+*X*) transitions, where *X* denotes up to 8 eight states below or above the HOMO and LUMO states, respectively. Dashed lines indicate that the higher energy part of spectra are not converged because only at most *X* transitions were included. The thin arrows indicate the onset of the spectra.

The relaxed NPs exhibited an intragap state within a well-defined electronic gap. The formation of an intragap state was a persistent feature within the entire range of diameters studied here, and for all choices of initial configurations (see Supporting Information for details). Although the intragap state is unoccupied in neutral dots and it is formally the LUMO, we used the notation of LUMO for the orbital right above the intragap state. Figure 1 illustrates a $Cd_{33}Se_{33}$ NP model along with the wave functions corresponding to the HOMO, intragap and LUMO states. Our results on IGSs are consistent with our earlier work,[34] and with that of the group of Prezhdo on $Cd_{33}Se_{33}$,[45] as well as with the study of smaller $Cd_{20}Se_{19}$.[46] However, these earlier works did not address the significance of this state for solar applications.

Figure 2 shows the HOMO, LUMO, and the IntraGap State (IGS) as a function of size, for the CdSe NPs studied here. The HOMO−LUMO gap varies from 2.6 to 1.5 eV as the NP size increases, and the LUMO−IGS energy difference varies from 0.6 to 0.4 eV. Although HOMO−LUMO gaps do not correspond to optical gaps, their trends as a function of size are qualitatively representative of those of optical gaps, if one assumes (at least partial) cancellation between quasi-particle corrections to Kohn−Sham eigenvalues and exciton binding energies.[47] In terms of absolute values, Kohn−Sham gaps have a tendency to underestimate optical gaps.[48,49] Using the data of Jasieniak *et al.*,[44] we found that the ≈2.5 eV gap of the d = 1.5 nm CdSe is indeed an underestimate of the optical gap for this size; our computed gap at d = 1.5 nm would correspond instead to the experimental one for NPs with diameter of 2−2.5 nm. With these cautionary remarks, these NP energies can be used to estimate the maximum achievable solar cell efficiency using the results of ref 50. We estimated ≈40% efficiency under one-sun conditions for the largest CdSe NP, well in excess of the Shockley−Quiesser limit.

Partial Filling and Optical Absorption in Intragap States. Once an IGS is formed, it will support *all* the optical absorption processes necessary for an IB solar cell, if the IGS is partially filled and if its optical transitions are dipole active.

To investigate the optical activity of the IGS, we computed the oscillator strength of the HOMO−*X*→LUMO+*X*, HOMO−*X*→IGS, and IGS→LUMO+*X* transitions, where *X* denotes up to 8 states below or above the HOMO and LUMO states, respectively. Figure 3 shows the computed absorption for three different NPs. Our findings for the trends in the absorption can be summarized as follows. (1) The IGS → LUMO transition was always optically active. (2) With the exception of the smallest NP, the HOMO→IGS and HOMO→LUMO transitions were also always optically active. At the edge of the spectrum, the oscillator strengths were often lower than that of the IGS→LUMO transitions, but they grew rapidly with increasing energy, becoming comparable to the oscillator strengths of the IGS→LUMO transition at energies ≈0.5 eV above the band edge transitions.

Partial filling of the IGS may be achieved either by photodoping or by charge doping. In the case of photodoping, the IGS of solar cells that is empty in the initial state may be partially filled by photons with subgap energies.[51] Since the IB conversion efficiency increases with the filling fraction of the IGS, photodoping-based IB solar cells are best suited for concentrating PV designs.[52] Efficiencies in the 25−41% range were calculated for 10−1000 sun concentrations.[53] For such photodoped PV designs, the above-described CNPs with IGSs can be readily adapted.

An alternative way to fill the IGS is by charge doping. The current status of electron/hole doping of CNPs is well summarized in ref 54. Charge doping techniques include electrochemical,[55] photochemical[56,57] and chemical doping.[58] CdSe CNPs were successfully electron doped by all of these methods.[37,59−62] PbSe CNPs were doped by cobaltocene, in a recent work by the Klimov group, where a well separated IGS was observed in nanoparticles prepared in solution.[35] The relevance of these observations for solar applications, however, was not articulated.

Building on the results of ref 35, we investigated the possibility of doping CdSe nanoparticles with cobaltocene. In the absence of solvents, electron transfer from the cobaltocene to the CdSe NPs may take place if the electron affinity (EA) of the nanoparticle (*i.e.*, the energy required to fill the IGS state) is larger than the ionization potential (IP) of the molecule. We thus computed these two quantities using ΔSCF techniques.

Figure 4 shows the vertical −EAs of the CdSe NP as a function of size. Quantum confinement effects decrease −EA with increasing NP diameter. While the trend of −EA as a function of size is the same as that of the IGS single particle energy (*cf.*, Figure 2), their absolute values do not coincide. For example, in $Cd_{45}Se_{45}$, the single particle IGS energy is ≈−4.1 eV, while −EA is ≈−3.2 eV. Adiabatic effects tend to decrease −EA by 0.1−0.2 eV. Our results for the −EAs of the $Cd_{33}Se_{33}$ NPs (varying between 3.0 and 3.1 eV, depending on the structural model) are in very good agreement with those of recent *ab initio* calculations,[63] that reported a value of 3.1 eV for −EA of the $Cd_{33}Se_{33}$ NP, using the B3LYP functional. To verify the robustness of our approach, we also calculated the −EA of $Cd_{15}Se_{15}$ NP using the hybrid functional PBE0 and found a value that differs from the PBE one by only 0.2 eV.

Turning to the calculation of the IP, we recall that cobaltocene is an organometallic compound, consisting of a Co atom sandwiched between two carbon rings. Cobaltocene has two conformations: the eclipsed one, with D_{5h} symmetry, and the staggered one with D_{5d} symmetry.[64] The unpaired electron of the Co atom occupies a doubly degenerate orbital, making cobaltocene a Jahn−Teller (JT) unstable doublet.[65,66] This instability drives the molecule to develop a static JT distortion, with an energy gain of

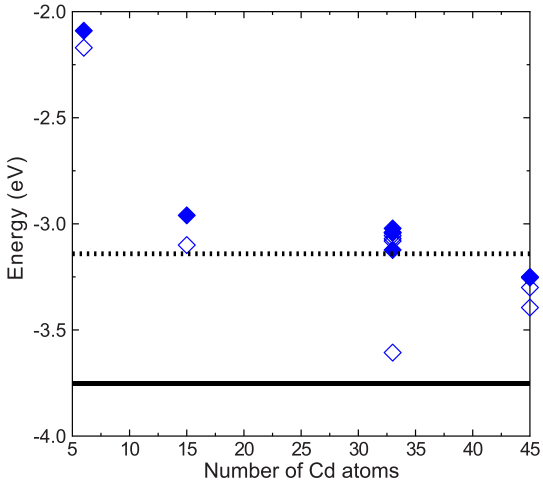

Figure 4. Theoretical vertical (filled diamonds) and adiabatic (empty diamonds) electron affinities (EA) of CdSe NP as a function of the number of atoms in the NP. The EA values were obtained from total energy differences (ΔSCF) between the neutral NP and the NP with an extra electron in the IGS, computed within DFT-PBE. Also shown are the experimental reduction potentials (E^0) of two reducing agents: cobaltocene (solid black line) and decamethylcobaltocene (dotted black line).

about 1.4 eV. We found that in vacuum, in the JT distorted ground state, the vertical −IP of cobaltocene was −5.33 eV within the PBE approximation and −5.45 eV when using the PBE0 functional. Both values are within 10% of the reported experimental values of −5.55 eV (from UPS studies)[67] and −5.44 eV (from a zero kinetic-energy technique).[68] The cobaltocene family contains an even stronger reducing agent, decamethylcobaltocene, having a higher experimental vertical −IP of −4.71 eV.[67] Our calculated −IP is −4.25 eV, again within 10% error.

The results reported above showed that in the absence of solvents, both cobaltocene and decamethylcobaltocene molecules are not suitable to dope the IGS of the CdSe NPs studied here. However, the presence of a solvent may play a crucial role in facilitating doping. In this case, the key quantity determining the electron transfer from the dopant is the solvation corrected −IP, the reduction potential E^0 of the cobaltocene/cobaltocenium redox couple. Thus, cobaltocene is predicted to dope the NPs if its reduction potential E^0 is above the −EA of the NPs.

Experimentally, the E^0 of cobaltocene is −3.75 eV,[36] close to the range required to dope the CdSe NPs considered here; that of decamethylcobaltocene is higher, E^0 = −3.14 eV,[36] and above the vertical −EA of −3.2 eV of the $Cd_{45}Se_{45}$ NP, as shown in Figure 4. We note that the reduction potentials of cobaltocene and decamethylcobaltocene are reported to be largely solvent independent.[36]

To determine if the NP may indeed be doped, the reduction potential of the dopant has to be compared with the solvent-corrected −EA of the NP. Recent

theoretical studies using continuum solvation models showed that the −EA of the $Cd_{33}Se_{33}$ NP decreases by about 0.2 eV both in toluene and in acetonitrile, in favor of electron transfer.[63] In sum, our results showed that CdSe nanoparticles in solution in the size range considered here (with 90 atoms, *i.e.*, with a diameter of 1.5 nm or larger) may be doped by decamethylcobaltocene.

Additional effects can be exploited to dope the CdSe nanoparticles. These include choosing ligands with suitable dipole moments to tune the band edges.[69,70] Some of these ligands were theoretically predicted to shift the band edges of CdSe surfaces by as much as 1−2 eV.[71] Recent experiments showed that by carefully choosing the capping ligand of CdSe NPs their ionization potential can be tuned by few tenths of an electronvolt.[44,72] Finite temperature fluctuations, neglected in our calculations, may also help bring the −EA below the redox potential of the dopant molecules.[73]

The preceding discussion shows that several physical mechanisms are available to fill the IGS of CdSe NPs, thereby activating the IB-mediated absorption processes.

Nanoparticle Array: Band Formation. For solar applications, the CNPs must be arranged into an absorber array with a spatial extent comparable to the absorption length. This typically involves forming a "closed-packed NP assembly",[32] a "NP film",[35,54] a "NP-solid",[59] or a "NP superlattice".[33] These CNP−arrays are synthesized starting from a colloidal solution. In ref 35, *p*−*n* diodes were formed by retaining the CNPs in their solvent, and encapsulating the entire array between LiF/Al and NiO electrodes. A widely studied class of Grätzel cells also involves NPs in electrolytes.[74] In other designs. the solvents are dried out of the array to form solid structures.[54] This strategy was specifically implemented for CdSe CNPs.[32,33,75] In what follows, we propose a concept of CNPIB solar cell for solvent-containing arrays.

The organization of CNPs into an array is important to provide an absorbing volume and a path for extracting the photogenerated charges. In such an array, the IGSs may combine into an IB with a finite width. Luque−Martí proposed that there is an optimal IB width that minimizes the undesirable nonradiative recombination due to the delocalization of the IGSs.[76] On the other hand, recently, Krich argued that the IGSs may relocalize in the recombination process.[77] While the ideal IB width is yet unsettled, an essential prerequisite is to understand the formation of IBs in CNP arrays. An other critical aspect of recombination in NP arrays is extensively analyzed in ref 78. One of the main messages of that work was that it is possible to tune the ratio of radiative and nonradiative recombination rates by the engineering of the strain on the NP−host boundary, providing a promising pathway to minimize the unwanted nonradiative recombination.

For an initial assessment, we studied NP arrays of CdSe NPs without ligands and solvent. Such arrays have been recently fabricated in ref 79 where the NPs were stripped of the ligands. We built simple cubic (SC) and face-centered cubic (FCC) NP arrays from representative $Cd_{15}Se_{15}$ NPs, determined their band structure (shown in Figure 5) using the PBE functional, and analyzed the formation of an IB.

First, we verified that our NP arrays are bound. The binding energies were ≈0.16 eV/NP for the SC and ≈0.24 eV/NP for the FCC arrays, showing that NP solids in the absence of ligands are not only bound but stable at room temperature.

Figure 5 shows the IB width (defined as the difference between the maximum and minimum of the energy of the IB) of the SC and FCC arrays of $Cd_{15}Se_{15}$ NPs as a function of the NP−NP distance for a specific relative orientation of the NPs.[80] The fact that we found substantial IB widths suggests that the IGS of individual NPs is not strongly localized. To measure the IGS localization and those of states close to the HOMO and LUMO, we computed their Inverse Participation Ratio (IPR): we recall that the higher the IPR, the more localized a state. Indeed, we found small IPRs for unoccupied states, including the IGS and relatively high IPRs for occupied states close to the HOMO. For example, the ratio of the IPR of the HOMO and that of the IGS in $Cd_{33}Se_{33}$ is ≈5, indicating that the IGS is less localized than the HOMO. We observed similar relative localization of states for all the CdSe NPs studied here (Supporting Information Figure S2). Such a delocalization of the IGS state may help reducing the unwanted nonradiative recombination according to the Luque−Martí scenario.[76]

The NP−NP distance may be controlled by attaching ligands of suitable length to the NPs.[31] However, these same ligands may also alter the formation and presence of IGSs.[81] Therefore, the engineering of the ligands should be guided by two interdependent criteria: avoid the suppression of the IGS formed in bare NPs and yield a NP−NP spacing leading to the desired IB width. As an example, the nominal length of the shortest routinely used organic ligand, EDT, is ≈4 Å. Figure 5 shows that at that distance, which translates to a lattice constant of ≈13.25 Å, the IB width is about ≈0.2 eV.

Encouragingly, some recent experimental evidence points to the formation of bands in NP arrays.[75,82,83] These papers reported high mobilities for NP arrays, which in some cases were temperature independent. Yet other experiments showed that "mid-gap" states can form weakly conducting bands in PbS NPs.[84] Although PbS may be used, in principle, to realize the intermediate band concept, it has too small of a gap.

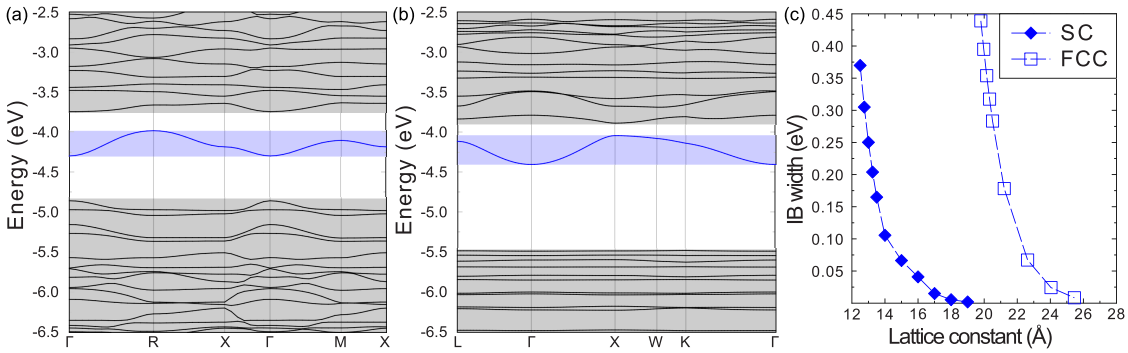

Figure 5. Band structure of a simple-cubic (SC) (a) and a face-centered cubic (FCC) (b) $Cd_{15}Se_{15}$ NP array along high-symmetry lines computed at the theoretical equilibrium lattice constant of ≈12.75 and ≈20.15 Å. The closest NP−NP distance is ≈3.5 and ≈3.3 Å between two Se atoms in the SC and FCC structures, respectively. (c) The width of the IB, defined as the difference between the maximum and the minimum of the band energies, in SC and FCC arrays of $Cd_{15}Se_{15}$ NPs, as a function of the lattice constant.

The formation of a coherent IB can be ensured by using monodisperse NPs. Techniques to synthesize monodisperse CdSe NPs are already available,[32,85] leading to an average diameter of 4 nm and standard deviation of less than 5%.[86,87] Remarkably, "magic cluster" CdSe NPs were synthesized with a practically monodisperse size distribution.[88]

We note that most colloidally synthesized II−VI nanoparticles are cation-rich. Since our NPs are stoichiometric, our results are strictly valid only for stoichiometric NPs. However, cation-rich NPs are charge balanced by the extra charge provided by the ligands,[89,90] and thus, one may expect that stoichiometric bare NPs are good approximation to charge-balanced cation-rich NPs. We carried out a preliminary exploration on a cation-rich but charge balanced structural model adopted from the literature.[91] We found a well separated intragap state for the deprotonated acetic acid covered $Cd_{32}Se_{22}$ NP, ≈0.5 eV below the LUMO, similar to what we have found for our surface reconstructed and stoichiometric NPs. This suggests that our stoichiometric nanoparticles may indeed be a good approximation to cation rich and charged balanced NPs.

Core−shell NPs are also promising to realize IBs in CNP arrays. Recently, the successful synthesis of CdSe/CdS[92] and CdSe/ZnS core−shell NPs with high level of monodispersity was reported.[87]

We close with some considerations about charge extraction. Extraction of electrons and holes from the IB reduces the open circuit voltage V_{oc} of a solar cell device, and thus, it is to be avoided. This could be accomplished, for example, by forming a charge-selective extraction layer next to the metallic electrodes.[93] Finding extraction layers with favorable band alignment to the CBM and VBM of the intermediate band CdSe NP absorber will be the subject of future investigations. However, some initial insight can be gained by a recent study on CdSe NP sensitized solar cells whose results indicate that TiO_2 might be a potential candidate as an electron extraction layer for the IB-CdSe NPs studied here.[94]

CONCLUSION

In this Article, we proposed a new paradigm for IB solar cells. Using the results of first-principles calculations, we proposed that colloidal nanoparticles (CNPs) are a promising platform for implementing the IB concept in solar cells. We focused on CdSe CNPs and showed that in arrays of surface reconstructed CdSe dots IB states well separated from the valence and conduction band edges are formed. These bands may be chemically doped, *e.g.*, using decamethylcobaltocene in solution, thereby activating IB-induced absorption processes.

The recent reports of close to 10% efficient CNP solar cell prove the maturity of the CNP technology.[38,39] Hence, it may soon become possible to fabricate the proposed colloidal nanoparticle intermediate band solar cells with reasonable technical effort.

We close by articulating a broad vision and context for the present work. CNPs have been put forward as a promising platform to boost the solar cell efficiency in the high energy portion of the solar spectrum *via* Multiple Exciton Generation (MEG). The present work points to the exciting possibility of using CNPs for boosting the cell efficiency in the low energy portion of the solar spectrum by forming an Intermediate Band. Motivated by these twin observations, we envision the possibility of a "Full Spectrum Boost" for solar cells by developing CNPs that *simultaneously* allow for MEG and IB mechanisms' enhancements of solar energy conversion. We propose that CNPs are uniquely suited to implement such a Full Spectrum Boost.

We also note that implementing both IB and MEG in the same NPs may give rise to promising synergies as well. While MEG was indeed observed in NPs, its onset was at high energies, thus possibly undermining its

overall utility for solar applications. Therefore, if the NPs are modified to simultaneously having an additional IB inside their gap, then the MEG onset may occur at more favorable energies.

METHODS

We performed our computations using density functional theory as implemented in the Quantum-ESPRESSO[95] code. We used plane wave basis sets and projector augmented wave pseudopotentials[96,97] and treated the following electrons as part of the valence partition: Cd, $4s^2 4p^6 4d^{10} 5s^2$; Co, $3s^2 3p^6 3d^7 4s^2$; and Se, $4s^2 4p^4$. We used a wave function (charge density) energy cutoff of 80 (800) Ry. We verified that these cutoffs were sufficient to converge ionization potentials and electron affinities within 0.02 eV. Most of our calculations were carried out using the generalized gradient approximation with the PBE exchange-correlation functional,[98] and a series of specific tests to assess the robustness of our results were performed with the PBE0 functional.[99] The PBE0 calculations were carried out by using norm-conserving pseudopotentials with a wave function cutoff of 150 Ry.

Vertical electron affinities (EA) and ionization potentials (IP) of the isolated NPs were calculated by computing total energy differences between ionized and neutral configurations at the geometry of the neutral NP geometry (ΔSCF method). In our calculations, the NPs were separated by at least 10 Å. *Adiabatic* electron affinities and ionization potentials were obtained as total energy differences between ionized and neutral configurations at the respective, optimized geometries.

The convergence of the total energy as a function of cell size for the charged isolated NPs was tested by increasing the NP−NP separation of the $Cd_{15}Se_{15}$ NP from 10 to 15 Å and by applying the Makov−Payne correction scheme.[100] Absolute single particle energies were computed with respect to the vacuum level, by determining the average electrostatic potential at the cell boundary and again by applying Makov−Payne-like corrections.

Conflict of Interest: The authors declare no competing financial interest.

Acknowledgment. The authors thank A. Martí, A. Nozik, J. Krich, S. Hubbard, A. Freundlich, J. Skone, T. Szilvási for useful discussions and N. Brawand for rendering the nanoparticle solid image. M.V. thanks A. Csuhai for inspiring discussions. This research was supported by the NSF Solar Collaborative under DMR-1035468. This research used resources of the National Energy Research Scientific Computing Center (NERSC) through the NISE project Larnint. NERSC is supported by the Office of Science of the U.S. Department of Energy under Contract No. DE-AC02-05CH11231. The authors also acknowledge support from the Center for Advanced Solar Photophysics (CASP), an Energy Frontier Research Center (EFRC) funded by the US Department of Energy (DOE), Office of Science, Office of Basic Energy Sciences (BES).

Supporting Information Available: Density of states, inverse participation ratio for CdSe NPs and definition of oscillator strengths. The Supporting Information is available free of charge on the ACS Publications website at DOI: 10.1021/acsnano.5b00332.

REFERENCES AND NOTES

1. Shockley, W.; Queisser, H. J. Detailed Balance Limit of Efficiency of p-n Junction Solar Cells. *J. Appl. Phys.* **1961**, *32*, 510–519.
2. Green, M. *Third Generation Photovoltaics: Advanced Solar Energy Conversion*; Springer Series in Photonics; Springer: Berlin, 2006.
3. Nozik, A. J. Spectroscopy and Hot Electron Relaxation Dynamics in Semiconductor Quantum Wells and Quantum Dots. *Annu. Rev. Phys. Chem.* **2001**, *52*, 193.
4. Luque, A.; Martí, A. Increasing the Efficiency of Ideal Solar Cells by Photon Induced Transitions at Intermediate Levels. *Phys. Rev. Lett.* **1997**, *78*, 5014–5017.
5. Wolf, M. Limitations and Possibilities for Improvement of Photovoltaic Solar Energy Converters Part I: Considerations for Earth's Surface Operation. *Proc. IRE* **1960**, *48*, 1246–1263.
6. Keevers, M. J.; Green, M. A. Efficiency Improvements of Silicon Solar Cells by the Impurity Photovoltaic Effect. *J. Appl. Phys.* **1994**, *75*, 4022–4031.
7. Nozik, A. J. Quantum Dot Solar Cells. *Physica E* **2002**, *14*, 115–120.
8. Hanna, M. C.; Nozik, A. J. Solar Conversion Efficiency of Photovoltaic and Photoelectrolysis Cells with Carrier Multiplication Absorbers. *J. Appl. Phys.* **2006**, *100*, 074510.
9. Bremner, S. P.; Levy, M. Y.; Honsberg, C. B. Limiting Efficiency of an Intermediate Band Solar Cell under a Terrestrial Spectrum. *Appl. Phys. Lett.* **2008**, *92*, 171110.
10. Semonin, O. E.; Luther, J. M.; Choi, S.; Chen, H.-Y.; Gao, J.; Nozik, A. J.; Beard, M. C. Peak External Photocurrent Quantum Efficiency Exceeding 100% *via* MEG in a Quantum Dot Solar Cell. *Science* **2011**, *334*, 1530–1533.
11. Zhai, G.; Church, C. P.; Breeze, A. J.; Zhang, D.; Alers, G. B.; Carter, S. A. Quantum Dot $PbS_{0.9}Se_{0.1}/TiO_2$ Heterojunction Solar Cells. *Nanotechnology* **2012**, *23*, 405401.
12. Klimov, V. I. Multicarrier Interactions in Semiconductor Nanocrystals in Relation to the Phenomena of Auger Recombination and Carrier Multiplication. *Annu. Rev. Condens. Matter Phys.* **2014**, *5*, 285–316.
13. Beard, M. C.; Luther, J. M.; Semonin, O. E.; Nozik, A. J. Third Generation Photovoltaics Based on Multiple Exciton Generation in Quantum Confined Semiconductors. *Acc. Chem. Res.* **2013**, *46*, 1252–1260.
14. Shabaev, A.; Hellberg, C. S.; Efros, A. L. Efficiency of Multiexciton Generation in Colloidal Nanostructures. *Acc. Chem. Res.* **2013**, *46*, 1242–1251.
15. Padilha, L. A.; Stewart, J. T.; Sandberg, R. L.; Bae, W. K.; Koh, W.-K.; Pietryga, J. M.; Klimov, V. I. Carrier Multiplication in Semiconductor Nanocrystals: Influence of Size, Shape, and Composition. *Acc. Chem. Res.* **2013**, *46*, 1261–1269.
16. Jaeger, H. M.; Hyeon-Deuk, K.; Prezhdo, O. V. Exciton Multiplication from First Principles. *Acc. Chem. Res.* **2013**, *46*, 1280–1289.
17. Vörös, M.; Rocca, D.; Galli, G.; Zimanyi, G. T.; Gali, A. Increasing Impact Ionization Rates in Si Nanoparticles through Surface Engineering: A Density Functional Study. *Phys. Rev. B* **2013**, *87*, 155402.
18. Wippermann, S.; Vörös, M.; Rocca, D.; Gali, A.; Zimanyi, G.; Galli, G. High-Pressure Core Structures of Si Nanoparticles for Solar Energy Conversion. *Phys. Rev. Lett.* **2013**, *110*, 046804.
19. Vörös, M.; Wippermann, S.; Somogyi, B.; Gali, A.; Rocca, D.; Galli, G.; Zimanyi, G. T. Germanium Nanoparticles with Non-Diamond Core Structures for Solar Energy Conversion. *J. Mater. Chem. A* **2014**, *2*, 9820.
20. Govoni, M.; Marri, I.; Ossicini, S. Carrier Multiplication between Interacting Nanocrystals for Fostering Silicon-Based Photovoltaics. *Nat. Photonics* **2012**, *6*, 672–679.
21. Martí, A.; Cuadra, L.; Luque, A. Quantum Dot Intermediate Band Solar Cell. *Conf. Rec. IEEE Photovoltaic Spec. Conf.* **2000**, 940–943.
22. Martí, A.; López, N.; Antolín, E.; Cánovas, E.; Stanley, C.; Farmer, C.; Cuadra, L.; Luque, A. Novel Semiconductor Solar Cell Structures: The Quantum Dot Intermediate Band Solar Cell. *Thin Solid Films* **2006**, *511−512*, 638–644.
23. Martí, A.; Antolín, E.; Stanley, C. R.; Farmer, C. D.; López, N.; Díaz, P.; Cánovas, E.; Linares, P. G.; Luque, A. Production of Photocurrent due to Intermediate-to-Conduction-Band

Transitions: A Demonstration of a Key Operating Principle of the Intermediate-Band Solar Cell. *Phys. Rev. Lett.* **2006**, *97*, 247701.
24. Hubbard, S. M.; Cress, C. D.; Bailey, C. G.; Raffaelle, R. P.; Bailey, S. G.; Wilt, D. M. Effect of Strain Compensation on Quantum Dot Enhanced GaAs Solar Cells. *Appl. Phys. Lett.* **2008**, *92*, 123512.
25. Laghumavarapu, R. B.; Moscho, A.; Khoshakhlagh, A.; El-Emawy, M.; Lester, L. F.; Huffaker, D. L. GaSb/GaAs Type II Quantum Dot Solar Cells for Enhanced Infrared Spectral Response. *Appl. Phys. Lett.* **2007**, *90*, 173125.
26. Wang, W.; Lin, A. S.; Phillips, J. D. Intermediate-Band Photovoltaic Solar Cell Based on ZnTe:O. *Appl. Phys. Lett.* **2009**, *95*, 011103.
27. Ertekin, E.; Winkler, M. T.; Recht, D.; Said, A. J.; Aziz, M. J.; Buonassisi, T.; Grossman, J. C. Insulator-to-Metal Transition in Selenium-Hyperdoped Silicon: Observation and Origin. *Phys. Rev. Lett.* **2012**, *108*, 026401.
28. Sullivan, J. T.; Simmons, C. B.; Krich, J. J.; Akey, A. J.; Recht, D.; Aziz, M. J.; Buonassisi, T. Methodology for Vetting Heavily Doped Semiconductors for Intermediate Band Photovoltaics: A Case Study in Sulfur-Hyperdoped Silicon. *J. Appl. Phys.* **2013**, *114*, 103701.
29. Cirloganu, C. M.; Padilha, L. A.; Lin, Q.; Makarov, N. S.; Velizhanin, K. A.; Luo, H.; Robel, I.; Pietryga, J. M.; Klimov, V. I. Enhanced Carrier Multiplication in Engineered Quasi-Type-II Quantum Dots. *Nat. Commun.* **2014**, *5*, 4148.
30. Santra, P. K.; Kamat, P. V. Mn-Doped Quantum Dot Sensitized Solar Cells: A Strategy to Boost Efficiency over 5%. *J. Am. Chem. Soc.* **2012**, *134*, 2508–2511.
31. Liu, Y.; Gibbs, M.; Puthussery, J.; Gaik, S.; Ihly, R.; Hillhouse, H. W.; Law, M. Dependence of Carrier Mobility on Nanocrystal Size and Ligand Length in PbSe Nanocrystal Solids. *Nano Lett.* **2010**, *10*, 1960–1969.
32. Murray, C. B.; Kagan, C. R.; Bawendi, M. G. Synthesis and Characterization of Monodisperse Nanocrystals and Close-packed Nanocrystal Assemblies. *Annu. Rev. Mater. Sci.* **2000**, *30*, 545–610.
33. Zaitseva, N.; Dai, Z. R.; Leon, F. R.; Krol, D. Optical Properties of CdSe Superlattices. *J. Am. Chem. Soc.* **2005**, *127*, 10221–10226.
34. Puzder, A.; Williamson, A. J.; Gygi, F.; Galli, G. Self-healing of CdSe Nanocrystals: First-Principles Calculations. *Phys. Rev. Lett.* **2004**, *92*, 217401.
35. Koh, W.-k.; Koposov, A. Y.; Stewart, J. T.; Pal, B. N.; Robel, I.; Pietryga, J. M.; Klimov, V. I. Heavily Doped n-Type PbSe and PbS Nanocrystals Using Ground-State Charge Transfer from Cobaltocene. *Sci. Rep.* **2013**, *3*, 2004.
36. Connelly, N. G.; Geiger, W. E. Chemical Redox Agents for Organometallic Chemistry. *Chem. Rev.* **1996**, *96*, 877–910.
37. Rinehart, J. D.; Schimpf, A. M.; Weaver, A. L.; Cohn, A. W.; Gamelin, D. R. Photochemical Electronic Doping of Colloidal CdSe Nanocrystals. *J. Am. Chem. Soc.* **2013**, *135*, 18782–18785.
38. Chuang, C.-H. M.; Brown, P. R.; Bulović, V.; Bawendi, M. G. Improved Performance and Stability in Quantum Dot Solar Cells through Band Alignment Engineering. *Nat. Mater.* **2014**, *13*, 796–801.
39. Labelle, A. J.; Thon, S. M.; Masala, S.; Adachi, M. M.; Dong, H.; Farahani, M.; Ip, A. H.; Fratalocchi, A.; Sargent, E. H. Colloidal Quantum Dot Solar Cells Exploiting Hierarchical Structuring. *Nano Lett.* **2015**, *15*, 1101–1108.
40. Mendes, M. J.; Hernández, E.; López, E.; García-Linares, P.; Ramiro, I.; Artacho, I.; Antolín, E.; Tobías, I.; Martí, A.; Luque, A. Self-Organized Colloidal Quantum Dots and Metal Nanoparticles for Plasmon-Enhanced Intermediate-Band Solar Cells. *Nanotechnology* **2013**, *24*, 345402.
41. Wippermann, S.; Vörös, M.; Gali, A.; Gygi, F.; Zimanyi, G. T.; Galli, G. Solar Nanocomposites with Complementary Charge Extraction Pathways for Electrons and Holes: Si Embedded in ZnS. *Phys. Rev. Lett.* **2014**, *112*, 106801.
42. Mendes, M. J.; Luque, A.; Tobías, I.; Martí, A. Plasmonic Light Enhancement in the Near-Field of Metallic Nanospheroids for Application in Intermediate Band Solar Cells. *Appl. Phys. Lett.* **2009**, *95*, 071105.
43. Jasieniak, J.; Smith, L.; Embden, J. v.; Mulvaney, P.; Califano, M. Re-examination of the Size-Dependent Absorption Properties of CdSe Quantum Dots. *J. Phys. Chem. C* **2009**, *113*, 19468–19474.
44. Jasieniak, J.; Califano, M.; Watkins, S. E. Size-Dependent Valence and Conduction Band-Edge Energies of Semiconductor Nanocrystals. *ACS Nano* **2011**, *5*, 5888–5902.
45. Kilina, S. V.; Kilin, D. S.; Prezhdo, O. V. Breaking the Phonon Bottleneck in PbSe and CdSe Quantum Dots: Time-Domain Density Functional Theory of Charge Carrier Relaxation. *ACS Nano* **2009**, *3*, 93–99.
46. Wang, L.-W.; Zunger, A. Pseudopotential Calculations of Nanoscale CdSe Quantum Dots. *Phys. Rev. B* **1996**, *53*, 9579–9582.
47. Delerue, C.; Lannoo, M.; Allan, G. Excitonic and Quasiparticle Gaps in Si Nanocrystals. *Phys. Rev. Lett.* **2000**, *84*, 2457–2460.
48. Williamson, A. J.; Grossman, J. C.; Hood, R. Q.; Puzder, A.; Galli, G. Quantum Monte Carlo Calculations of Nanostructure Optical Gaps: Application to Silicon Quantum Dots. *Phys. Rev. Lett.* **2002**, *89*, 196803.
49. Puzder, A.; Williamson, A. J.; Grossman, J. C.; Galli, G. Surface Chemistry of Silicon Nanoclusters. *Phys. Rev. Lett.* **2002**, *88*, 097401.
50. Bremner, S. P.; Levy, M. Y.; Honsberg, C. B. Limiting Efficiency of an Intermediate Band Solar Cell under a Terrestrial Spectrum. *Appl. Phys. Lett.* **2008**, *92*, 171110.
51. Sullivan, J.; Simmons, C.; Buonassisi, T.; Krich, J. Targeted Search for Effective Intermediate Band Solar Cell Materials. *IEEE J. Photovoltaics* **2015**, *5*, 212–218.
52. Strandberg, R.; Reenaas, T. Optimal Filling of the Intermediate Band in Idealized Intermediate-Band Solar Cells. *IEEE Trans. Electron Devices* **2011**, *58*, 2559–2565.
53. Strandberg, R.; Reenaas, T. W. Drift-Diffusion Model for Intermediate Band Solar Cells Including Photofilling Effects. *Prog. Photovoltaics* **2011**, *19*, 21–32.
54. Engel, J. H.; Alivisatos, A. P. Postsynthetic Doping Control of Nanocrystal Thin Films: Balancing Space Charge to Improve Photovoltaic Efficiency. *Chem. Mater.* **2014**, *26*, 153–162.
55. Wehrenberg, B. L.; Guyot-Sionnest, P. Electron and Hole Injection in PbSe Quantum Dot Films. *J. Am. Chem. Soc.* **2003**, *125*, 7806–7807.
56. Rinehart, J. D.; Weaver, A. L.; Gamelin, D. R. Redox Brightening of Colloidal Semiconductor Nanocrystals Using Molecular Reductants. *J. Am. Chem. Soc.* **2012**, *134*, 16175–16177.
57. Schimpf, A. M.; Gunthardt, C. E.; Rinehart, J. D.; Mayer, J. M.; Gamelin, D. R. Controlling Carrier Densities in Photochemically Reduced Colloidal ZnO Nanocrystals: Size Dependence and Role of the Hole Quencher. *J. Am. Chem. Soc.* **2013**, *135*, 16569–16577.
58. Engel, J. H.; Surendranath, Y.; Alivisatos, A. P. Controlled Chemical Doping of Semiconductor Nanocrystals Using Redox Buffers. *J. Am. Chem. Soc.* **2012**, *134*, 13200–13203.
59. Yu, D.; Wang, C.; Guyot-Sionnest, P. N-Type Conducting CdSe Nanocrystal Solids. *Science* **2003**, *300*, 1277–1280.
60. Shim, M.; Guyot-Sionnest, P. N-Type Colloidal Semiconductor Nanocrystals. *Nature* **2000**, *407*, 981–983.
61. Wang, C.; Shim, M.; Guyot-Sionnest, P. Electrochromic Nanocrystal Quantum Dots. *Science* **2001**, *291*, 2390–2392.
62. Boehme, S. C.; Wang, H.; Siebbeles, L. D.; Vanmaekelbergh, D.; Houtepen, A. J. Electrochemical Charging of CdSe Quantum Dot Films: Dependence on Void Size and Counterion Proximity. *ACS Nano* **2013**, *7*, 2500–2508.
63. Kuznetsov, A. E.; Beratan, D. N. Structural and Electronic Properties of Bare and Capped $Cd_{33}Se_{33}$ and $Cd_{33}Te_{33}$ Quantum Dots. *J. Phys. Chem. C* **2014**, *118*, 7094–7109.
64. While in our calculations the eclipsed conformation was 0.22 eV more stable than the staggered one, there was only a minuscule difference between the calculated ionization potentials of the two conformations.

65. Zlatar, M.; Schläpfer, C.-W.; Penka Fowe, E.; Daul, C. A. Density Functional Theory Study of the Jahn-Teller Effect in Cobaltocene. *Pure Appl. Chem.* **2009**, *81*, 1397–1411.
66. We confirmed that the quartet ground state is more than 10 eV higher in energy for both conformations.
67. Cauletti, C.; Green, J. C.; Kelly, M.; Powell, P.; van Tilborg, J.; Robbins, J.; Smart, J. Photoelectron Spectra of Metallocenes. *J. Electron Spectrosc. Relat. Phenom.* **1980**, *19*, 327–353.
68. Ketkov, S. Y.; Selzle, H. L. Threshold Ionization of Cobaltocene: The Metallocene Molecule Revealing Zero Kinetic Energy States. *Angew. Chem., Int. Ed.* **2012**, *51*, 11527–11530.
69. Brown, P. R.; Kim, D.; Lunt, R. R.; Zhao, N.; Bawendi, M. G.; Grossman, J. C.; Bulovic, V. Energy Level Modification in Lead Sulfide Quantum Dot Thin Films through Ligand Exchange. *ACS Nano* **2014**, *8*, 5863.
70. Li, Y.; O'Leary, L. E.; Lewis, N. S.; Galli, G. Combined Theoretical and Experimental Study of Band-Edge Control of Si through Surface Functionalization. *J. Phys. Chem. C* **2013**, *117*, 5188–5194.
71. Yang, S.; Prendergast, D.; Neaton, J. B. Tuning Semiconductor Band Edge Energies for Solar Photocatalysis *via* Surface Ligand Passivation. *Nano Lett.* **2012**, *12*, 383–388.
72. Bloom, B. P.; Zhao, L.-B.; Wang, Y.; Waldeck, D. H.; Liu, R.; Zhang, P.; Beratan, D. N. Ligand-induced Changes in the Characteristic Size-Dependent Electronic Energies of CdSe Nanocrystals. *J. Phys. Chem. C* **2013**, *117*, 22401–22411.
73. Opalka, D.; Pham, T. A.; Sprik, M.; Galli, G. The Ionization Potential of Aqueous Hydroxide Computed Using Many-Body Perturbation Theory. *J. Chem. Phys.* **2014**, *141*, 034501.
74. O'Regan, B.; Grätzel, M. A. Low-Cost, High-Efficiency Solar Cell Based on Dye-sensitized Colloidal TiO_2 Films. *Nature* **1991**, *353*, 737–740.
75. Choi, J.-H.; Fafarman, A. T.; Oh, S. J.; Ko, D.-K.; Kim, D. K.; Diroll, B. T.; Muramoto, S.; Gillen, J. G.; Murray, C. B.; Kagan, C. R. Bandlike Transport in Strongly Coupled and Doped Quantum Dot Solids: A Route to High-Performance Thin-Film Electronics. *Nano Lett.* **2012**, *12*, 2631–2638.
76. Luque, A.; Martí, A.; Antolín, E.; Tablero, C. Intermediate Bands *versus* Levels in Non-Radiative Recombination. *Phys. B: Condensed Matter* **2006**, *382*, 320–327.
77. Krich, J. J.; Halperin, B. I.; Aspuru-Guzik, A. Nonradiative Lifetimes in Intermediate Band Photovoltaics—Absence of Lifetime Recovery. *J. Appl. Phys.* **2012**, *112*, 013707.
78. Brawand, N. P.; Vörös, M.; Galli, G. Surface Dangling Bonds Are a Cause of B-Type Blinking in Si Nanoparticles. *Nanoscale* **2015**, *7*, 3737–3744.
79. Rosen, E. L.; Sawvel, A. M.; Milliron, D. J.; Helms, B. A. Influence of Surface Composition on Electronic Transport through Naked Nanocrystal Networks. *Chem. Mater.* **2014**, *26*, 2214–2217.
80. The NP geometry has been held fixed while changing the distance between nanoparticles. This is a good approximation as long as the NPs are far apart from each other so that there is no direct chemical bonding between them.
81. Puzder, A.; Williamson, A. J.; Zaitseva, N.; Galli, G.; Manna, L.; Alivisatos, A. P. The Effect of Organic Ligand Binding on the Growth of CdSe Nanoparticles Probed by *ab Initio* Calculations. *Nano Lett.* **2004**, *4*, 2361–2365.
82. Liu, Y.; Tolentino, J.; Gibbs, M.; Ihly, R.; Perkins, C. L.; Liu, Y.; Crawford, N.; Hemminger, J. C.; Law, M. PbSe Quantum Dot Field-Effect Transistors with Air-Stable Electron Mobilities above 7 $cm^2\ V^{-1}s^{-1}$. *Nano Lett.* **2013**, *13*, 1578–1587.
83. Lee, J.-S.; Kovalenko, M. V.; Huang, J.; Chung, D. S.; Talapin, D. V. Band-like Transport, High Electron Mobility and High Photoconductivity in All-Inorganic Nanocrystal Arrays. *Nat. Nanotechnol.* **2011**, *6*, 348–352.
84. Nagpal, P.; Klimov, V. I. Role of Mid-Gap States in Charge Transport and Photoconductivity in Semiconductor Nanocrystal Films. *Nat. Commun.* **2011**, *2*, 486.
85. Murray, C. B.; Norris, D. J.; Bawendi, M. G. Synthesis and Characterization of Nearly Monodisperse CdE (E = Sulfur, Selenium, Tellurium) Semiconductor Nanocrystallites. *J. Am. Chem. Soc.* **1993**, *115*, 8706–8715.
86. Peng, Z. A.; Peng, X. Formation of High-Quality CdTe, CdSe, and CdS Nanocrystals Using CdO as Precursor. *J. Am. Chem. Soc.* **2001**, *123*, 183–184.
87. Talapin, D. V.; Rogach, A. L.; Kornowski, A.; Haase, M.; Weller, H. Highly Luminescent Monodisperse CdSe and CdSe/ZnS Nanocrystals Synthesized in a Hexadecylamine-Trioctylphosphine Oxide-Trioctylphospine Mixture. *Nano Lett.* **2001**, *1*, 207–211.
88. Park, Y.-S.; Dmytruk, A.; Dmitruk, I.; Kasuya, A.; Okamoto, Y.; Kaji, N.; Tokeshi, M.; Baba, Y. Aqueous Phase Synthesized CdSe Nanoparticles with Well-defined Numbers of Constituent Atoms. *J. Phys. Chem. C* **2010**, *114*, 18834–18840.
89. Voznyy, O.; Zhitomirsky, D.; Stadler, P.; Ning, Z.; Hoogland, S.; Sargent, E. H. A Charge-Orbital Balance Picture of Doping in Colloidal Quantum Dot Solids. *ACS Nano* **2012**, *6*, 8448–8455.
90. Kim, D.; Kim, D.-H.; Lee, J.-H.; Grossman, J. C. Impact of Stoichiometry on the Electronic Structure of PbS Quantum Dots. *Phys. Rev. Lett.* **2013**, *110*, 196802.
91. Margraf, J. T.; Ruland, A.; Sgobba, V.; Guldi, D. M.; Clark, T. Theoretical and Experimental Insights into the Surface Chemistry of Semiconductor Quantum Dots. *Langmuir* **2013**, *29*, 15450–15456.
92. Li, J. J.; Wang, Y. A.; Guo, W.; Keay, J. C.; Mishima, T. D.; Johnson, M. B.; Peng, X. Large-Scale Synthesis of Nearly Monodisperse CdSe/CdS Core/Shell Nanocrystals Using Air-Stable Reagents *via* Successive Ion Layer Adsorption and Reaction. *J. Am. Chem. Soc.* **2003**, *125*, 12567–12575.
93. Kramer, I. J.; Sargent, E. H. The Architecture of Colloidal Quantum Dot Solar Cells: Materials to Devices. *Chem. Rev.* **2014**, *114*, 863–882.
94. Robel, I.; Kuno, M.; Kamat, P. V. Size-Dependent Electron Injection from Excited CdSe Quantum Dots into TiO_2 Nanoparticles. *J. Am. Chem. Soc.* **2007**, *129*, 4136–4137.
95. Giannozzi, P.; Baroni, S.; Bonini, N.; Calandra, M.; Car, R.; Cavazzoni, C.; Ceresoli, D.; Chiarotti, G. L.; Cococcioni, M.; Dabo, I.; et al. QUANTUM ESPRESSO: a Modular and Open-Source Software Project for Quantum Simulations of Materials. *J. Phys.: Condens. Matter* **2009**, *21*, 395502.
96. Blöchl, P. E. Projector Augmented-Wave Method. *Phys. Rev. B* **1994**, *50*, 17953–17979.
97. Kresse, G.; Joubert, D. From Ultrasoft Pseudopotentials to the Projector Augmented-Wave Method. *Phys. Rev. B* **1999**, *59*, 1758–1775.
98. Perdew, J. P.; Burke, K.; Ernzerhof, M. Generalized Gradient Approximation Made Simple. *Phys. Rev. Lett.* **1996**, *77*, 3865–3868.
99. Adamo, C.; Barone, V. Toward Reliable Density Functional Methods without Adjustable Parameters: The PBE0 Model. *J. Chem. Phys.* **1999**, *110*, 6158–6170.
100. Makov, G.; Payne, M. C. Periodic Boundary Conditions in *ab Initio* Calculations. *Phys. Rev. B* **1995**, *51*, 4014–4022.